Title
Performance evaluation of an energy tuning assembly for neutron spectral shaping

Authors
Bevins, James E
Sweger, Z
Munshi, N
et al.

Publication Date
2019-04-01

DOI
10.1016/j.nima.2019.01.049

Peer reviewed

Nuclear Inst. and Methods in Physics Research, A 923 (2019) 79–87

Contents lists available at ScienceDirect

Nuclear Inst. and Methods in Physics Research, A

journal homepage: www.elsevier.com/locate/nima

Performance evaluation of an energy tuning assembly for neutron spectral shaping

James E. Bevins [a,*], Z. Sweger [b], N. Munshi [b], B.L. Goldblum [c], J.A. Brown [c], D.L. Bleuel [d], L.A. Bernstein [c], R.N. Slaybaugh [c]

[a] Department of Engineering Physics, Air Force Institute of Technology, Wright Patterson Air Force Base, OH 45433, USA
[b] Department Physics, University of California, Berkeley, CA 94720, USA
[c] Department of Nuclear Engineering, University of California, Berkeley, CA 94720, USA
[d] Lawrence Livermore National Laboratory, Livermore, CA 94550, USA

ARTICLE INFO

Keywords:
Neutron energy tuning
Beam shaping
Neutron activation analysis
Spectrum unfolding
Fast neutrons
Surrogate debris

ABSTRACT

An energy tuning assembly (ETA) was designed to be fielded at the National Ignition Facility (NIF) to modify the characteristic D-T fusion spectrum to include a prompt fission neutron spectral component. The ETA was characterized at the 88-Inch Cyclotron at Lawrence Berkeley National Laboratory to measure the shaped spectrum from an incident deuteron breakup neutron source, test the proposed neutron spectroscopy techniques used to inform the flux measurements at NIF, and validate the ability to predict ETA performance using a Monte Carlo Neutral Particle (MCNP) simulation. Activation foils (i.e., Ni, In, Au, Al) were exposed to a collimated 33-MeV deuteron-breakup beam originating from a tantalum breakup target. The source spectrum absent the ETA was characterized using a set of activation foils and the STAYSL unfolding code. Finally, the ETA-modified spectrum was obtained using activation foil unfolding with a $\frac{\chi^2}{\nu} = 0.92$. The ETA-modified unfolded spectrum agreed with the MCNP-simulated prediction in the energy range of 0.1–14 MeV, but exhibited disagreements in the 10 eV–100 keV region. This work demonstrates shaping of the NIF neutron spectrum via the ETA to be a viable path forward for tailored neutron beams at NIF.

1. Introduction

Very early on, it was deemed desirable to modify neutron spectra for basic and applied scientific research and development. By 1935, only three years after the discovery of the neutron, hydrogen thermalization and cadmium filters were employed to modify or remove portions of neutron spectra [1,2]. Over 80 years later, neutron spectral modification techniques have not changed significantly.

Neutron filters, sometimes called neutron screens, have been used in a wide variety of nuclear science and engineering applications. In activation analysis, highly absorbing filters employing Cd, B, Gd, Hf, etc. are often used to suppress the thermal neutron flux allowing for epi-thermal reactions to dominate [3]. Materials science and nuclear physics have used neutron filters on cold neutron beams to filter neutrons with wavelengths less than the critical wavelength, resulting in a high purity, low energy beam [4,5]. To certify epi-thermal and fast reactor designs, solid and liquid neutron filters have been used for irradiation degradation and power transient studies, respectively [6]. In the field of radiation detection, filters have been used to enhance the gamma signal by suppressing high neutron fields and to selectively detect thermal and fast neutrons [7,8]. Neutron filters can also be used to produce quasi-monochromatic neutron beams with V, Mn, S, ^{56}Fe, or other nuclei that have deep interference minima [9]. Parametrically optimized, sometimes layered, neutron filter designs for several applications such as neutron radiography, boron neutron capture therapy, and neutron transmutation doping of silicon have also been developed by combining multiple elements from the list of applications above [10–12].

Recent research introduced the concept of an energy tuning assembly (ETA) using modern optimization techniques to advance the state-of-the-art for designing custom neutron spectra [13,14]. The first ETA was designed for the technical nuclear forensics (TNF) community to produce fission and activation products that provide the characteristic “fingerprint" used to aid in the attribution of the originating source of a detonated nuclear weapon (aka synthetic post-detonation debris) [15–17].

This work investigates the ability to model and measure the performance of the TNF ETA designed to be fielded at the National Ignition Facility (NIF) as a passive diagnostic with the desired neutron spectrum achieved across the small experimental cavity, labeled Element 6 in Fig. 1. The nature of the experiment and ETA design

* Corresponding author.
E-mail address: james.bevins@afit.edu (J.E. Bevins).

https://doi.org/10.1016/j.nima.2019.01.049
Received 26 November 2018; Accepted 15 January 2019
Available online 21 January 2019
0168-9002/Published by Elsevier B.V.

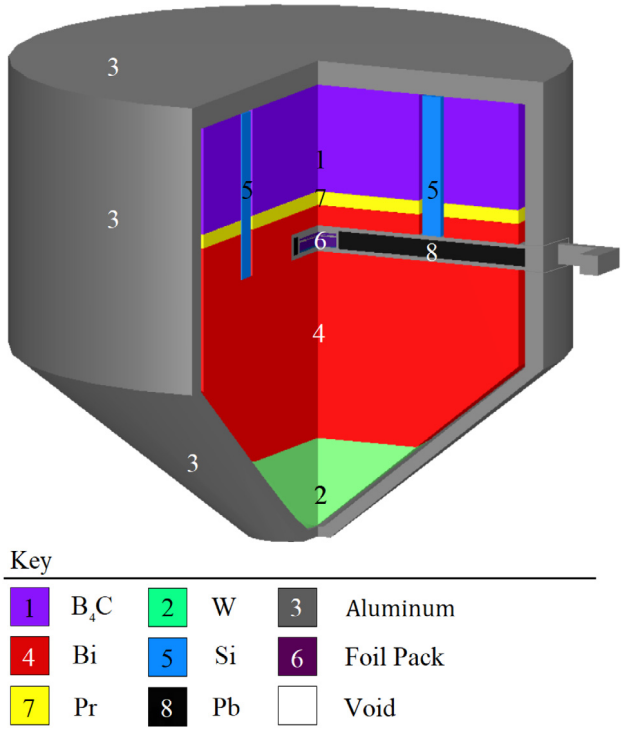

Fig. 1. ETA designed to generate a thermonuclear plus prompt fission spectrum at the National Ignition Facility [13].

limits the neutron spectroscopy options available to measure the neutron spectrum achieved in the cavity. While typical techniques such as time-of-flight [18], proton recoil spectrometers [19], pulse height spectrum unfolding with organic scintillators [20], and capture gated spectrometers [21] will not work, foil activation analysis and unfolding is a viable technique to measure the neutron energy spectrum in the ETA experimental cavity. Foil activation analysis for neutron spectrum unfolding is a well established method that has been used to measure spectra for reactors [22], the Spallation Neutron Source [23], spallation at the Isotope Production facility [24], ^{252}Cf [25], etc. For this work, the STAYSL PNNL code developed by Greenwood et al. was used to unfold the activation results [26].

Unfolding neutron spectra using foil activation analysis is often dependent on the initial *a priori* spectrum. This *a priori* spectrum is generally developed using a model of the system under consideration. However, modeling the ETA performance was considered a challenging proposition given the weighted impact of component cross-sections on the resulting spectrum modification that could highlight nuclear data deficiencies. Thus, the goal of this work was to validate the ability to model the ETA performance to address the concerns about the nuclear data impacts on the model. This was accomplished through a series of experiments at the 88-Inch Cyclotron at Lawrence Berkeley National Laboratory (LBNL).

The paper is organized as follows. Section 2 explains how the ETA was developed and the intended application as context for the current measurement. Section 3 describes how the 88-Inch Cyclotron at LBNL was used to measure the ETA performance in preparation for full implementation at the NIF. Section 4 describes the methods used to analyze the foil activation data, and Section 5 details the performance achieved. Concluding remarks are presented in Section 6.

2. Energy tuning assembly design

For the TNF application, the goal is to develop a spectrum that combines a D-T fusion, or thermonuclear (TN), plus a prompt fission neutron spectrum (PFNS) component [13]. For the purposes of brevity, this objective spectrum will be referred to as the TN+PFNS and is shown in Fig. 2. It is worth noting that this is a representative but notional TNF-relevant neutron spectrum, and there exists a variety of different neutron spectra that would be of interest for the purposes of generating synthetic debris. To avoid a man-power intensive “trial and error" approach to generating point designs, a software suite to automate the design of ETAs was developed. This resulted in the creation of a new optimization method, Gnowee [14], and a ETA design software, Coues [13].

These tools were used to create an ETA assembly to be fielded at the NIF as a proof of concept to generate synthetic debris. A cross-sectional view of the ETA design generated by Coeus for the TN+PFNS objective spectrum with NIF-imposed constraints of weight (75 kg), efficiency (1×10^9 fissions), and outer design envelope (to avoid 1ω scattered light) is shown in Fig. 1. The outer diameter is 280 mm, the overall length is 240.2 mm, and the central sample cavity is 8.93 mm tall with a diameter of 53.1 mm.[1] The ETA was built by American Elements.

The ETA, as designed, will only generate a TN+PFNS when exposed to a source neutron spectrum similar to the NIF D-T fusion neutron spectrum. However, validation of the ability to model the results and unfold the neutron spectrum can be carried out using a surrogate facility. For this purpose, exploratory experiments were conducted at the 88-Inch Cyclotron to determine the ability to model and measure the performance of the ETA as a developmental step toward creating synthetic post-detonation fission products at the NIF.

3. Experimental setup

3.1. Beam design

The LBNL 88-Inch Cyclotron is capable of accelerating deuterons up to a maximum energy of 65 MeV with maximum currents on the order of 10 μA [27]. Deuterons, with a neutron separation energy of 2.22 MeV, are weakly bound and will produce neutrons via breakup in the Coulombic field of a heavier nucleus (elastic breakup), proton stripping reactions (inelastic breakup), and pre-equilibrium and evaporation emission from the excited compound nucleus formed by deuteron absorption [28–31]. Each production mechanism produces neutrons with different angular and energy distributions. The elastic and inelastic breakup reactions result in neutron distributions that are highly forward peaked with an average energy of

$$E_n = \frac{1}{2}\left(E_d - \frac{Ze^2}{R_{bu}} - Q\right), \tag{1}$$

where R_{bu} is the breakup radius, E_d is the energy of the deuteron, and Q is the Q value of the reaction, Z is the atomic number of the target nucleus, and e is the elementary charge of a electron (proton) [29,30].

Eq. (1) describes the downward shift in the peak and average neutron energy with increasing Z of the breakup target. The neutron distribution is narrows with increasing Z due to the higher dE/dZ of the heavier target nucleus and the increasing relative fraction of the elastic channels [29,32,33]. In contrast, the pre-equilibrium and evaporative emission channels will be roughly isotropic and have energy distributions peaked at much lower energies based on the characteristic temperature of the nucleus [31,33,34]. As the neutron emission angle increases, the relative contribution of the pre-equilibrium and evaporative emission channels increase, and the resulting energy distribution is far broader and less intense [31–33,35].

This diversity in neutron spectra as a function of incoming deuteron energy, outgoing angle, and the target enables the 88-Inch Cyclotron to be used to perform a variety of neutron related experiments. For the ETA experiments, a beam was designed to have a neutron spectrum that is

[1] Full mechanical drawing are available from https://github.com/SlaybaughLab/NIF_TNF_ETA/tree/master/AsConstructed/CAD_Models/AssemblyDrawings.

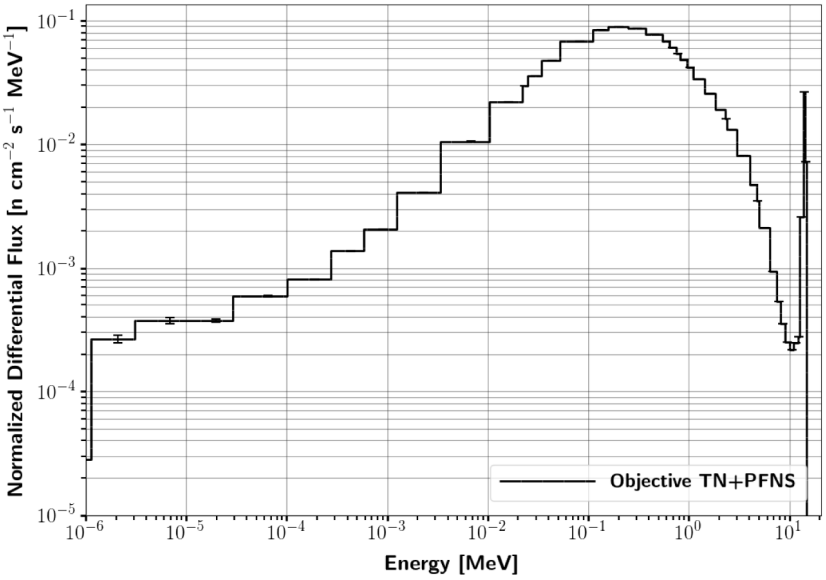

Fig. 2. TN+PFNS derived for use as the objective spectrum for ETA optimization and design [13].

peaked near 14 MeV—NIF-relevant energies thereby probing the same interaction mechanisms—and with as limited a high energy component as possible (~2% of the total spectrum is above 20 MeV). This was accomplished using a $^{2}H^{+}$ beam accelerated to 33 MeV and directed at a tantalum breakup target.

3.2. Foil irradiation

The deuteron beam was run at a current of ~8.2 μA during the foil irradiation for the measurement of the source beam and ~10.8 μA during the ETA foil irradiation. The Cave 0 beam line was optically aligned using a phosphor located in the Cave 0-1 beam box shown in Fig. 3 [27]. A Faraday cup was located at the breakup target location shown in Section 3 and equipped with a 4-mm-thick tantalum breakup target placed in the Cave 0 beam line [30,36]. The tantalum target was backed by a 14.5-mm-thick copper cooling assembly with a 38-mm-radius cutout centered on the tantalum target. The resulting neutrons entering the Cave 0-2 experimental area were collimated by ~1.5 m of concrete and ~1.5 m of concrete and sand bags encasing the beam pipe, producing a high contrast, open-air neutron beam. [27].

The origin is taken as beam line center (BLC) in the y and z directions, and the Cave 0-2 side of the Cave 0-1/Cave 0-2 wall shown in Fig. 3 in the x direction. The activation foils for both measurements were placed at BLC and 708.3 cm from the front face of the breakup target (~61 cm from origin). This resulted in a neutron flux of $\sim 3.6 \times 10^{5}$ n s^{-1} cm^{-2} at the experimental location, which is approximately seven orders of magnitude below the NIF source fluence, $\sim 5.7 \times 10^{12}$ n s^{-1} cm^{-2}, for which the ETA was designed. Some of this difference is compensated for in run time, but the drastically reduced flux places a limit on the experimental analysis techniques as described further in Section 4.

Three sets of activation foils were irradiated during this experiment. The first set was irradiated to provide geometry and coincidence summing correction factors for the high purity germanium (HPGe) detector. The correction factors were necessary because of the non-ideal counting geometry (i.e., 50-mm-diameter foils placed 1 cm from the detector) that was used to compensate for the drastically reduced flux (as compared to the NIF experiment design) and other experimental constraints (e.g., count time and number of detectors). The second foil set was irradiated to measure the source spectrum. The third foil set was irradiated in the ETA sample cavity to measure the ETA-modified spectrum.[2] All three sets of foils are described further in Section 4.2.

[2] All experimental data are available at https://github.com/SlaybaughLab/88_Data/blob/master/Experiments/Activation/33MeVTa_25Apr/.

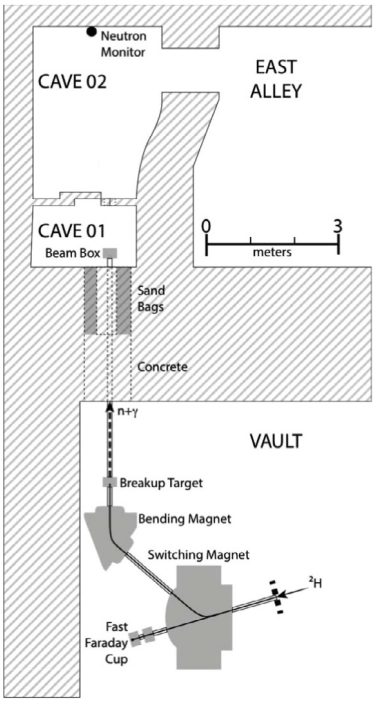

Fig. 3. Schematic representation of the 88-Inch Cyclotron vault and beam line to Cave 0. The Cave 0 experimental end station is comprised of two enclosures, Cave 0-1 and Cave 0-2, separated by a lead-lined door outfitted with a beam port.

3.3. Foil counting

Foil counting was conducted using the 88-Inch Cyclotron counting lab's Ortec coaxial HPGe GMX-50220-S detector. The detector has a 46.8% relative efficiency and was oriented in an upward facing direction in a lead lined case. An ORTEC ASPEC-927 multichannel analyzer with two 14-bit analog-to-digital converter (ADCs) was used to collect data and interface with MAESTRO software [37]. Efficiency calibration data were taken at positions 1 cm and 18 cm from the detector surface using the following sources and lines: ^{241}Am (59.54 keV), ^{133}Ba (80.998, 276.40, 302.85, and 356.01 keV), ^{137}Cs (661.657 keV), ^{60}Co (1173.23

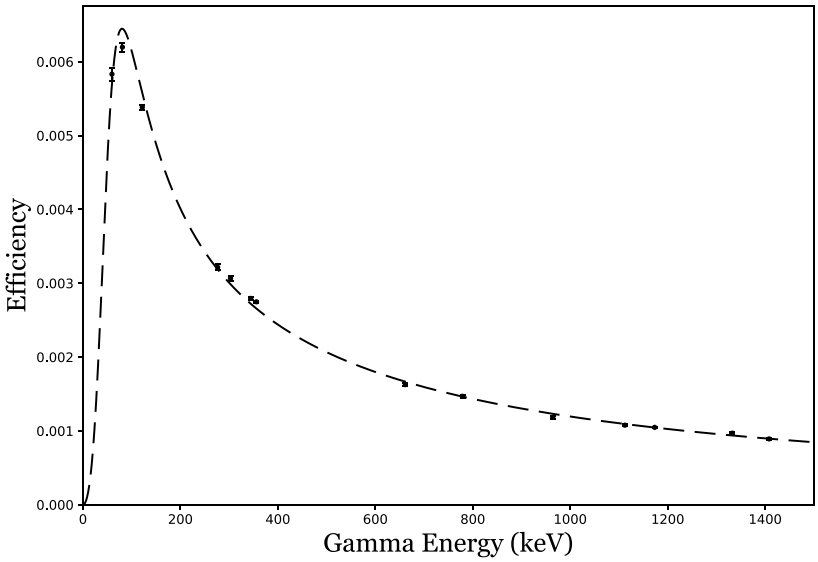

Fig. 4. HPGe efficiency calibration performed at 18 cm from the detector.

and 1332.49 keV), and ^{152}Eu (121.78, 244.70, 344.28, 778.90, 964.06, 1085.847, 1112.08, and 1408.01 keV). Additionally, ^{88}Y (392.87 and 1836.06 keV) and ^{88}Zr (898.04 keV) were used for energy-only calibration lines.

The efficiency function was calculated using a least squares method. On physical grounds, the efficiency curve asymptotically approaches a E_γ^{-1} relationship at high energy, so the inverse of the efficiencies was fit using a linear least squares regression with the basis vectors x, 1, $\frac{1}{x}$, $\frac{1}{x^2}$. The function, given by Eq. (2), was derived from fitting the experimental calibration data; the resulting chi-square per degrees of freedom between Eq. (2) and the experimental data was 2.6. The resulting efficiency curve and calibration data used are displayed in Fig. 4, where the error bars represent statistical and systematic uncertainty in the activity of each standard nuclide.

$$\epsilon_{18}(E_\gamma) = \frac{{E_\gamma}^2}{(0.677){E_\gamma}^3 + (168.92){E_\gamma}^2 - (15106.4)E_\gamma + 765419} \tag{2}$$

4. Analysis

4.1. Activation analysis

To perform a neutron spectrum unfold, the activity of each foil immediately following irradiation must be determined. The initial activity of a sample at the end of irradiation is given as:

$$A_0 = \frac{C(E_\gamma)\lambda e^{\lambda \Delta t_j}}{(1 - e^{-\lambda \Delta t_c})\epsilon_d(E_\gamma) f_l I_\gamma(E_\gamma)}, \tag{3}$$

where $C(E_\gamma)$ is the number of gamma-ray counts of a specific energy, E_γ, measured in the HPGe detector; λ is the decay constant of the nuclide responsible for emission of that gamma ray; Δt_j is the time between the end of irradiation and the start of the counting period; Δt_c is the total count time; $\epsilon_d(E_\gamma)$ is the efficiency of the detector at a given gamma-ray energy at a given distance, d, from the detector; f_l is the detector live-time fraction; and $I_\gamma(E_\gamma)$ is the intensity of gamma rays at that energy.

The source and ETA foil sets were both measured at a distance of 1 cm from the face of the detector, so the counting efficiency for these foils at 1 cm, $\epsilon_1(E_\gamma)$, is needed. However, at this distance correction factors must be applied to account for the geometry of the source and coincident summing from gamma cascades [38,39]. The measured absolute efficiency can be expressed as:

$$\epsilon_d(E_\gamma) = F_{d,\gamma} G_d(E_\gamma) \mathscr{E}_d(E_\gamma), \tag{4}$$

where $F_{d,\gamma}$ is the peak summing correction factor for a gamma ray characteristic of a given nuclide at some distance d from the detector, $G_d(E_\gamma)$ is the energy dependent geometric correction factor accounting for the efficiency difference between a volume source and a point source, and $\mathscr{E}_d(E_\gamma)$ is the intrinsic energy-dependent efficiency of the detector at a distance d.

At the counting location 1 cm from the detector, there can be large uncertainties in the calculated coincident summing and geometric correction factors. Therefore, it would be beneficial to express the initial activities in terms of the absolute efficiency 18 cm from the detector, $\epsilon_{18}(E_\gamma)$, instead of the absolute efficiency 1 cm from the detector, $\epsilon_1(E_\gamma)$. At large source-to-detector distances, the absolute efficiency is dominated by the $\mathscr{E}_d(E_\gamma)$ term since the foils approximate a point source, $G_{18}(E_\gamma) \approx 1$, and coincidence summing is negligible $F_d(\gamma) \approx 1$ [39]. At 18 cm from the detector, the absolute efficiency is approximately only a function of the gamma energy, with a minor geometric correction, $G_{18}(E_\gamma)$, required for the difference between a point source and the foil geometry. The latter correction was determined using MCNP [40].

Using a set of highly activated normalization foils corresponding to the same composition and geometry as the foils used to measure the source and ETA spectra, A_0 for a given decay can be calculated using Eq. (3) at a distance of 1 cm and 18 cm. Setting the initial activity equations at the two different distances equal to one another gives:

$$\frac{C_{1,\text{norm}}\lambda e^{\lambda \Delta t_{j(1\text{ cm})}}}{(1 - e^{-\lambda \Delta t_{c(1\text{ cm})}})\epsilon_1(E_\gamma) f_l I_\gamma} = \frac{C_{18,\text{norm}}\lambda e^{\lambda \Delta t_{j(18\text{ cm})}}}{(1 - e^{-\lambda \Delta t_{c(18\text{ cm})}})\epsilon_{18}(E_\gamma) f_l I_\gamma}, \tag{5}$$

which can be simplified to yield

$$\frac{C_{1,\text{norm}}}{C_{18,\text{norm}}} = \frac{\epsilon_1(E_\gamma)}{\epsilon_{18}(E_\gamma)}\kappa_{\text{norm}}, \tag{6}$$

where

$$\begin{aligned}\kappa_{norm} &= \frac{e^{\lambda \Delta t_{j(18\text{ cm})}}(1 - e^{-\lambda \Delta t_{c(1\text{ cm})}})}{e^{\lambda \Delta t_{j(1\text{ cm})}}(1 - e^{-\lambda \Delta t_{c(18\text{ cm})}})} \frac{f_{l(1\text{ cm})}}{f_{l(18\text{ cm})}} \\ &= e^{\lambda(\Delta t_{j(18\text{ cm})} - \Delta t_{j(1\text{ cm})})} \frac{(1 - e^{-\lambda \Delta t_{c(1\text{ cm})}})}{(1 - e^{-\lambda \Delta t_{c(18\text{ cm})}})} \frac{f_{l(1\text{ cm})}}{f_{l(18\text{ cm})}}.\end{aligned} \tag{7}$$

The total detector efficiency at 1 cm for each reaction channel can be related to the efficiency at 18 cm through the ratios of the counts for that reaction from the normalization data set by:

$$\epsilon_1(E_\gamma) = \frac{1}{\kappa_{norm}} \frac{C_{1,\text{norm}}}{C_{18,\text{norm}}} \epsilon_{18}(E_\gamma) G_{18}(E_\gamma). \tag{8}$$

Eq. (3) can be modified using Eq. (8) to express the initial activity from the sources and ETA irradiation data sets as a function of the efficiency

Table 1
Foil characteristics for all three measurements performed. The shorthand used is 1 = normalization foils, 2 = source spectrum measurement foils, and 3 = ETA spectrum measurement foils.

Foil	Diameter [mm]	Thickness [mm]	Weight [g]	Density [g cm^{-3}]	Elemental Purity
In1	49.8 ± 0.2	1.050 ± 0.025	14.461 ± 0.002	7.07	0.99999
In2	50.15 ± 0.10	1.021 ± 0.005	14.326 ± 0.002	7.10	0.99999
In3	50.05 ± 0.10	1.026 ± 0.010	14.47 ± 0.002	7.17	0.99999
Ni1	49.95 ± 0.05	1.040 ± 0.005	17.335 ± 0.002	8.51	0.9898
Ni2	49.50 ± 0.10	1.000 ± 0.003	16.934 ± 0.002	8.80	0.9898
Ni3	49.85 ± 0.10	1.003 ± 0.003	17.267 ± 0.002	8.82	0.9898
Au1	–	0.028 ± 0.002	0.278 ± 0.002	18.91	0.999
Au2	49.35 ± 0.10	0.094 ± 0.003	3.298 ± 0.002	18.34	0.999
Au3	49.35 ± 0.10	0.100 ± 0.003	3.542 ± 0.002	18.52	0.999
Al1	50.05 ± 0.10	1.020 ± 0.005	5.324 ± 0.002	2.65	0.99999
Al2	50.00 ± 0.10	1.013 ± 0.003	5.306 ± 0.002	2.67	0.99999
Al3	49.96 ± 0.10	1.010 ± 0.005	5.284 ± 0.002	2.67	0.99999

at 18 cm as:

$$A_0 = \frac{C_1(\gamma)\lambda e^{\lambda \Delta t_j}}{(1 - e^{-\lambda \Delta t_c})\epsilon_{18}(E_\gamma) G_{18} f_l I_\gamma} \frac{C_{18,\text{norm}}}{C_{1,\text{norm}}} \kappa_{\text{norm}}. \quad (9)$$

4.2. Irradiation foil measurement sets

To correct for geometry and coincident summing, a normalization foil pack was used to generate data for the method described in Section 4.1. The foil pack was irradiated for 16 min at ~8 μA using 33-MeV deuteron-breakup on a beryllium target plunged in the Cave 0-1 beam box. The foil pack was attached directly to the face of the beam box at BLC in the Cave 0-1 beam line. As the method is independent of the irradiation spectrum, this approach allowed for a quick, uniform irradiation that generated a high foil activity.

Each foil used in the measurement of the source or ETA spectra had an analog to correct for both geometry and coincidence summing. When possible, foils of the same elemental composition and size were used, but this was not possible for the gold (Au) foils where a 1 mil thick rectangular shaped foil (approximately 3 cm × 1.75 cm) was used for the normalization data. MCNP was used to determine geometry correction factors between the rectangular and the standard cylindrical foil geometries at 1 cm and 18 cm to enable use of the rectangular Au normalization foil to determine the coincidence summing correction factors.

A second foil pack, described in Table 1, was used to measure the source spectrum. The foil pack was irradiated for ~2.2 h at ~8.5 μA for a total integrated current of 64.32 mC. The foils were suspended in Cave 0-2 at the same location that they would be inside the ETA. This corresponded to a coordinate location of (61 cm, 0 cm, 0 cm) measured from the Cave 0-2 side of the Cave 0-1/0-2 wall in the x direction and from BLC for the y and z directions.

Finally, a third foil pack, described in Table 1, was used to measure the ETA-modified spectrum. The foil pack was irradiated for 19.5 h at ~12.0 μA for a total integrated current of 760.34 mC. The foils were placed in the sample irradiation cavity located in the ETA irradiation drawer shown in Fig. 1. This corresponded to a coordinate location of (61 cm, 0 cm, 0 cm) measured from the Cave 0-2 side of the Cave 0-1/0-2 wall in the x direction and from BLC for the y and z directions.

The foil characteristics are described in Table 1; for simplicity, each foil will be referred to by the shorthand name shown in the tables, where "1" is the normalization foil set, "2" is the source spectrum measurement, and "3" is the ETA spectrum measurement. Each foil was counted at 1 cm until 10,000 counts were achieved in the primary decay line associated with each reaction channel.

4.3. Monte Carlo simulations

Monte Carlo simulations of the ETA experimental setup were performed using MCNP v6.1.[3] A cross-sectional view of the 88-Inch Cyclotron Cave 0 experimental facility and beam line is shown in Fig. 5. Transport was modeled from the source generation point in the tantalum breakup target throughout the entire flight path to the ETA. Neutron transport was performed using a combination of ENDF/B-VII.1 libraries and MCNP's CEM03.03 models in the energy range where library data were not available [40]. Simulated activation of the foils was calculated using IRDFF v1.05 data libraries [41].

Published neutron spectra for 33 MeV deuteron breakup on tantalum (or similar energies) do not address the low energy component (<3 MeV) necessary for this measurement [30,32], so the measured deuteron-breakup source spectrum from this work was used as the initial source term for the ETA performance simulation. The model captures the first five degrees of the source from BLC, and simulations showed that neutrons emitted at angles greater than five degrees from BLC are negligible given the significant collimation and small solid angle subtended by the ETA. While the beam does vary in energy and intensity as a function of angle, previous research has shown the first five degrees to be roughly uniform [32]. The deviation from uniformity over this range has minimal impact on modeled results given the rapid fall off of neutron importance outside of the ~0.4° line of sight.

4.4. Spectrum unfolding

Unfolding of the activation results was accomplished using the STAYSL v1.2 suite [26] using the IRDFF v1.05 data libraries, which contain data for select reactions up to 60 MeV [41]. STAYSL is a neutron spectral adjustment code that finds the flux distribution using least-squares fitting methods. It is generally dependent on a reasonable *a priori* spectrum to generate an unfolded spectrum that is consistent with measured foil activities.

STAYSL has several modules available to account for correction factors due to self-shielding, decay, and burn-up. The SHIELD module was used to account for neutron self-shielding factors for non-threshold reactions, and the Sig-Phi Calculator was used to account for gamma self-shielding factors for all reactions. The Beam Correction Factor (BCF) module was used to correct for irradiation time history using the 88-Inch Cyclotron's beam current monitor (BCM). No burn-up correction factors were applied given the low reaction rates achieved.

The χ^2 statistic used by STAYSL for the least-squares minimization is given as [42]

$$\chi^2 = \begin{bmatrix} P - \bar{P} \\ A^\circ - \bar{A} \end{bmatrix}^\dagger \cdot \begin{bmatrix} N_P & 0 \\ 0 & N_{A^\circ} \end{bmatrix}^{-1} \cdot \begin{bmatrix} P - \bar{P} \\ A^\circ - \bar{A} \end{bmatrix}, \quad (10)$$

where A° is the foil activities, P is the neutron flux convolved with the cross-section, N_P is the co-variance matrix from the flux and nuclear data convolution, and N_{A° is the activity co-variance matrix.

5. Results and discussion

5.1. Beam measurement

The post-irradiation activities of the source spectrum measurement foils calculated from Eq. (9) are listed in Table 2. The activities listed here ignore gamma self-shielding as STAYSL corrects for this with its Sig-Phi Calculator [26]. For nuclides with multiple gamma rays with high branching ratios, the activity reported here is the average of the activities calculated using each gamma ray. While the ^{197}Au(n, γ)^{198}Au reaction has a metastable state, the contribution to the observed decays from metastable state feeding of the ground state during the counting period was negligible.

[3] The model of Cave 0 and the ETA are available at https://github.com/SlaybaughLab/88_Data/tree/master/Simulated/Activation/33MevTa/ETA/Model.

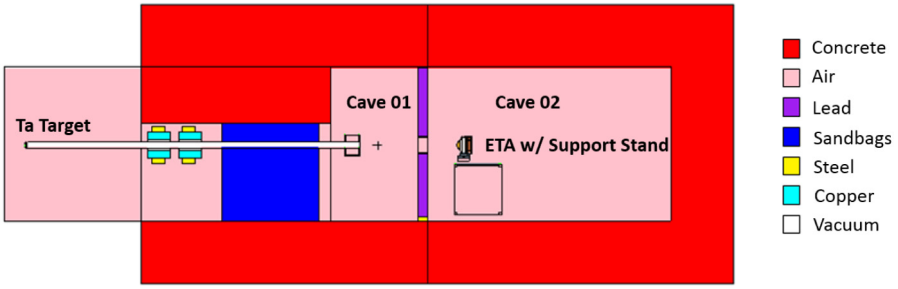

Fig. 5. Cross-sectional view of the MCNP model of the experimental configuration for the ETA measurement.

Table 2
A_0 from foils exposed to the unmodified 33 MeV deuteron breakup on Ta source spectrum with 64.32 mC of integrated current delivered over 7861 s.

Reaction	A_0 [Bq]
^{27}Al(n, α)^{24}Na	217.45 ± 2.78
^{27}Al(n,p)^{27}Mg	2628.50 ± 54.59
^{197}Au(n, γ)^{198}Au	18.46 ± 0.33
^{115}In(n,n')^{115m}In	1603.72 ± 13.21
^{115}In(n, γ)^{116m}In	5178.49 ± 56.05
^{58}Ni(n,2n)^{57}Ni	16.17 ± 0.23

Table 3
Measured, A_0, and simulated, $A_{0,sim}$ reaction product yields from foils exposed to the ETA modified 33 MeV deuteron breakup on Ta source spectrum with 760.34 mC of integrated current. All simulated results have less than 1% statistical uncertainty.

Reaction	A_0 [Bq]	$A_{0,sim}$ [Bq]	% Diff
^{27}Al(n, α)^{24}Na	376.26 ± 3.75	369.56	−1.78
^{27}Al(n,p)^{27}Mg	641.72 ± 18.37	667.20	−3.97
^{197}Au(n, γ)^{198}Au	142.52 ± 2.23	111.46	−21.79
^{115}In(n,n')^{115m}In	2,627.83 ± 25.19	2796.80	6.43
^{115}In(n, γ)^{116m}In	5,481.65 ± 90.75	3871.69	−29.37
^{58}Ni(n,2n)^{57}Ni	40.08 ± 0.51	42.06	−4.94

The *a priori* spectrum used was from a to-be-published unfolded pulse height spectrum measurement of the thick-target 33 MeV on tantalum deuteron breakup beam. The resulting normalized STAYSL unfolded deuteron breakup source spectrum is shown in comparison to the MCNP simulated ETA-modified spectrum in Fig. 6. The ETA MCNP simulation used the measured deuteron breakup spectrum from the STAYSL unfold as the transported starting source spectrum.

Although the starting source spectrum is significantly different than the NIF spectrum [13], similar spectral shaping characteristics can be observed in Fig. 6. First, the peak near 14 MeV is depopulated as it would be at the NIF. Second, the primary population of neutrons is in the PFNS range of energies that peak around 1 MeV. Finally, the ETA design limits the thermal and epi-thermal neutron population in the experimental cavity.

The measured deuteron breakup spectrum highlights some limitations of the foil pack used for this measurement. In general, there is overlapping and high sensitivity in the areas of high neutron flux as shown in Fig. 7. However, there is a gap in the 10 eV to 100 keV region. This region is below the threshold reactions and above the highly sensitive thermal region for the (n, γ) reactions. This means that the unfolded spectrum in this energy range is limited by the limited reaction sensitivity and is highly uncertain.

5.2. ETA measurement

The ETA-modified beam foil activities post-irradiation were calculated using Eq. (9) and are listed in Table 3. Again, the activities listed here ignore gamma self-shielding. The measured activation rates agree reasonably well with the simulated reaction rates. The largest differences are seen in the (n,γ) reactions where the initial source term is not well-defined.

The foil activation results in Table 3 were unfolded using STAYSL, the IRDFF v1.05 cross section library, and the *a priori* simulated spectrum shown in Fig. 6. The spectral adjustment resulted in a STAYSL calculated $\frac{\chi^2}{\nu} = 0.92$ between the measured activities and the activities calculated by convolving the unfolded flux with the IRDFF cross sections according to Eq. (10). The resulting STAYSL-unfolded ETA spectrum is shown in comparison to the MCNP-simulated ETA spectrum in Fig. 8.

A Pearson's Correlation Coefficient (PCC) was used to assess the overall correlation and shape match of the two spectra. The PCC was calculated to be 0.95 according to

$$r = \frac{n\sum x_i y_i - \left(\sum x_i \sum y_i\right)}{\sqrt{n\sum x_i^2 - \left(\sum x_i\right)^2}\sqrt{n\sum y_i^2 - \left(\sum y_i\right)^2}}, \tag{11}$$

where n is the sample size, x is the MCNP simulated spectra, and y is the STAYSL unfolded spectra. While this indicates a great overall correlation and shape match, the PCC does not account for magnitude shifts.

A Kolmogorov–Smirnov (KS) two-sample test does account for magnitude and can be used to provide a quantitative measure of the likelihood that the simulated and experimental data are representative of the same distribution according to

$$D = \max|\phi_{staysl}(E) - \phi_{mcnp}(E)|, \tag{12}$$

where $\phi_{STAYSL}(E)$ is the STAYSL unfolded flux spectrum and $\phi_{MCNP}(E)$ is the simulated flux spectrum. The KS two-sample test results in D=0.094, which has a p value of 0.66, indicating that the two spectra are consistent with coming from the same distribution. The largest differences noted in the MCNP model of the ETA are in the thermal and epi-thermal region where the (n, γ) reactions are sensitive to small changes in the overall flux. As before, the largest discrepancy between the modeled and simulated result is in the 10 eV to 10 keV region below the threshold reactions and above the high-cross section region (< 10 eV) for (n, γ) reactions. If the spectrum above 10 keV is used for the KS two-sample test, D=0.10, and the p is 0.78 – a stronger indication that the distributions are the same and the simulation is consistent with the measured spectrum.

6. Summary

An ETA was designed to produce a TN+PFNS at NIF through spectral modification techniques. This work sought to validate the ability to model the ETA using MCNP, a challenging proposition given the weighted impact of component cross-sections on the resulting spectrum modification that could highlight nuclear data deficiencies. Three sets of foil irradiation measurements were performed: normalization foils, foils with direct exposure to the deuteron breakup neutron source, and foils placed in the ETA experimental cavity to evaluate the shaped spectrum. The direct exposure foils were used to obtain an unfolded neutron spectrum that was used as the starting source spectrum in subsequent MCNP models to predict the ETA performance. The unfolded

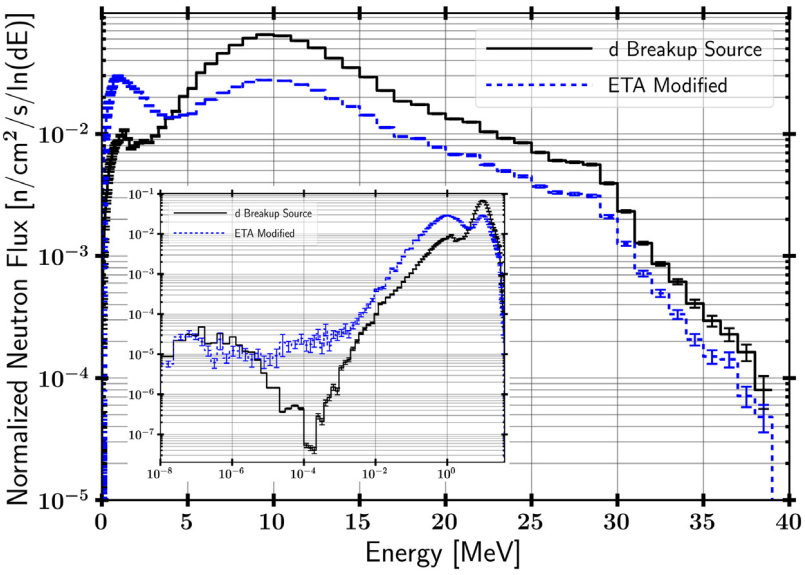

Fig. 6. Comparison of the STAYSL unfolded deuteron breakup source and the MCNP simulated ETA modified spectrum, which used the unfolded deuteron breakup source spectrum as the input source. The inset shows the same comparison on a log energy scale to highlight the changes at low energy.

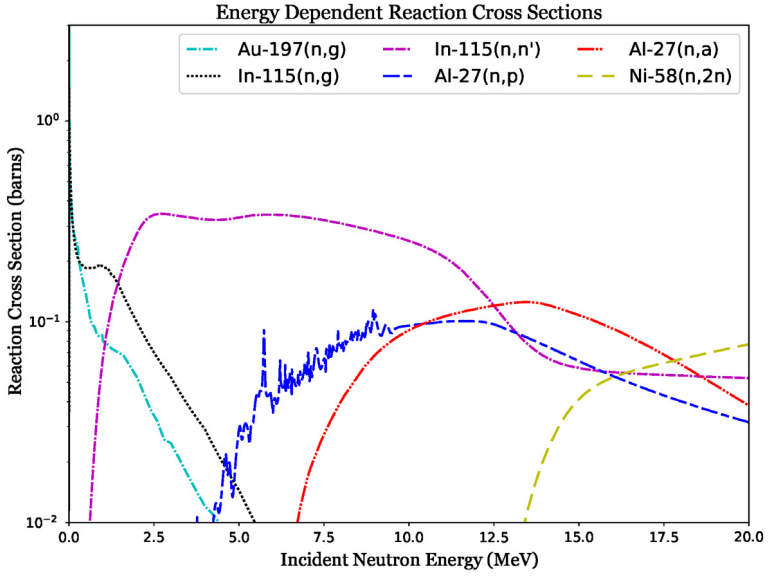

Fig. 7. IRDFF v1.05 cross-section data for the reactions used in the STAYSL unfold.

ETA-modified spectrum was obtained and compared with an MCNP simulated spectrum. The MCNP simulation models the ETA performance remarkably well over a large energy range and several orders of magnitude in response. The largest discrepancies between the model and the STAYSL unfolded spectrum are in the 10 eV to 10 keV region, where the activation foil pack had limited sensitivity and coverage.

This work demonstrates shaping of the NIF neutron spectrum via the ETA to be a viable path forward for tailored neutron beams at NIF. Importantly, this work validated the ability to model the TN+PFNS neutron spectrum produced by the proposed ETA, which allows for the use of foil activation spectroscopy requiring an known *a priori* spectrum to be used to unfold the neutron energy spectrum. Future validate of this spectral shaping methodology will be carried out at NIF to measure the ETA performance in producing the objective TN+PFNS spectrum.

Acknowledgments

The authors thank the 88-Inch Cyclotron operations and facilities staff for their help in performing these experiments. Thanks also to Ethan Boado, Matthew Harasty, Keegan Harrig, Will Kable, Thibault Laplace, Jørgen Mitbø, and Andrew Voyles for assistance with experimental execution. This material is based upon work supported in part by the Department of Energy National Nuclear Security Administration through the Nuclear Science and Security Consortium under Award Number DE-NA0003180, and performed under the auspices of the U.S. Department of Energy by Lawrence National Security, LLC, Lawrence Livermore National Laboratory under Contract DE-AC52-07NA27344. This work is also supported by the Lawrence Berkeley National Laboratory under Contract No. DE-AC02-05CH11231 for the US Nuclear Data Program and the National Science Foundation Graduate Research Fellowship under Grant No. NSF 11-582.

Disclaimer

The views expressed in this article are those of the authors and do not reflect the official policy or position of the United States Air Force, Department of Defense, or the U.S. Government.

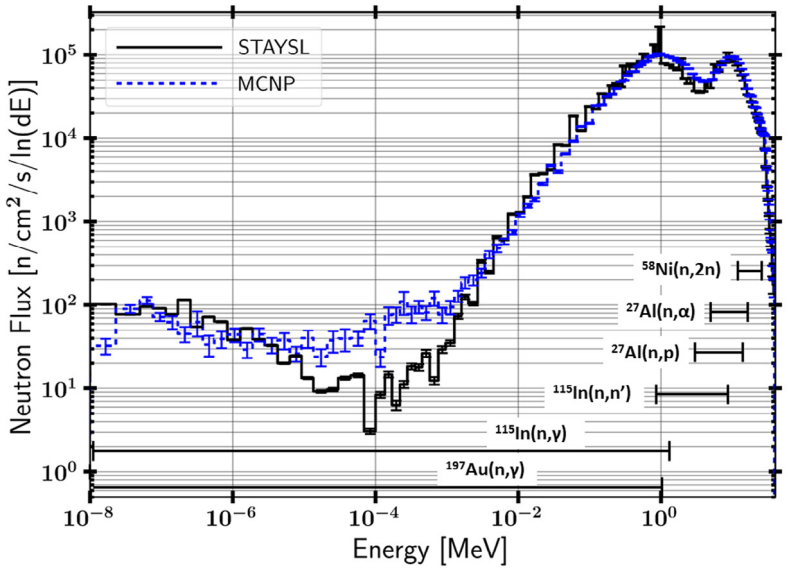

(a)

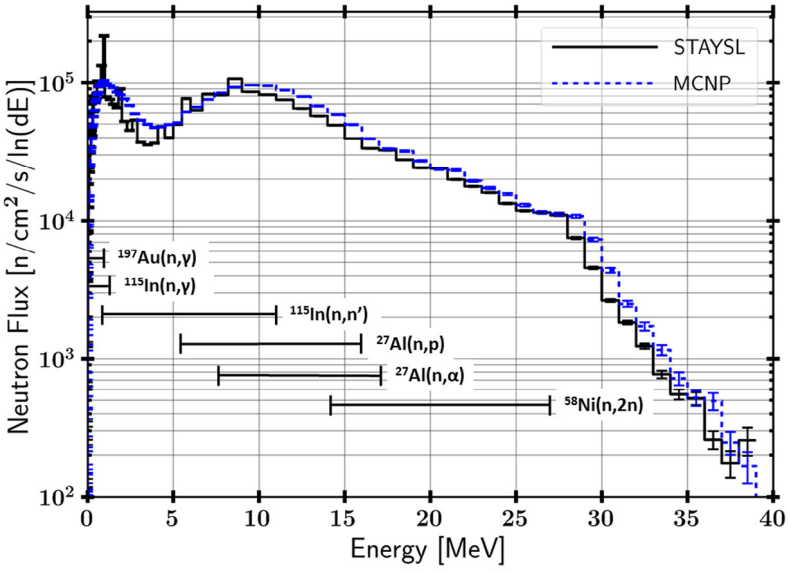

(b)

Fig. 8. Comparison of the STAYSL unfolded and MCNP simulated ETA modified spectrum in (a) log energy to emphasize the low energy region and (b) linear energy to emphasize the high energy region. The range shown for each reaction represents the 5%–95% activities range.

References

[1] J. Chadwick, M. Goldhaber, Disintegration by slow neutrons, Math. Proc. Camb. Phil. Soc. 31 (4) (1935) 612–616.

[2] J.R. Dunning, G.B. Pegram, G.A. Fink, D.P. Mitchell, Interaction of low energy neutrons with atomic nuclei, Phys. Rev. 47 (1935) 416–417.

[3] F. Rossitto, M. Terrani, S. Terrani, Choice of neutron filters in activation analysis, Nucl. Instrum. Methods (1972) 77–83.

[4] M. Adib, M. Kilany, On the use of bismuth as a neutron filter, Radiat. Phys. Chem. 66 (2) (2003) 81–88.

[5] P.A. Egelstaff, R.S. Pease, The design of cold neutron filters, J. Sci. Instrum. (1954) 207–212.

[6] N. Chrysanthopoulou, P. Savva, M. Varvayanni, N. Catsaros, Compilation of existing neutron screen technology, Sci. Technol. Nucl. Install. (2014).

[7] J.S. Brenizer, H. Berger, K.M. Gibbs, P. Mengers, C.T. Stebbings, D. Polansky, D.J. Rogerson, Development of a new electronic neutron imaging system, Nucl. Instrum. Methods Phys. Res. A 424 (1999) 9–14.

[8] V.G. Kiptilyi, a.V. Livke, V.I. Nagornyi, Y.Y. Nefedov, M.V. Savin, V.I. Semenov, V.a. Chirkin, Investigation of the parameters of neutron filters, Tech. Phys. 43 (4) (1998) 471–472.

[9] A. Murzin, V.P. Vertebnyi, V.I. Gavrilyuk, V. Libman, L.L. Litvinskii, Neutron filters based on V, Mn, S, and the stable isotopes 52Cr, 56Fe, 58Ni, and 60Ni, At. Energ. 67 (3) (1989) 216–218.

[10] H.-S. Kim, S.-Y. Oh, B.-J. Jun, M.-S. Kim, S. Chul -Gyo, H.-I. Kim, Design of a neutron screen for 6-inch neutron transmutation doping in hanaro, Nucl. Eng. Technol. 38 (7) (2006) 675–680.

[11] M. Mullner, H. Jex, Converter-thickness for optimum intensity in neutron-radiography, Nucl. Instrum. Methods 103 (1972) 229–233.

[12] D.L. Bleuel, R.J. Donahue, B.A. Ludewigt, J. Vujic, Designing accelerator-based epithermal neutron beams for boron neutron capture therapy, Med. Phys. 25 (9) (1998) 1725–1734.

[13] J. Bevins, Targeted modification of neutron energy spectra for national security applications (Ph.D. thesis), University of California, Berkeley, 2017.

[14] J. Bevins, R. Slaybaugh, Gnowee: a hybrid metaheuristic optimization algorithm for constrained, black box, combinatorial mixed-integer design, Nucl. Technol. (2018) http://dx.doi.org/10.1080/00295450.2018.1496692.

[15] 111th Congress, Nuclear forensics and attribution act, 2010.

[16] Joint Nuclear Forensics Working Group of the American Physical Society and the American Association for the Advancement of Science, Nuclear forensics: Role, state of the art, and program needs, Tech. rep., 2013.

[17] NTNFC, National Technical Nuclear Forensics (NTNF) Overview, 2015.
[18] V.Y. Glebov, T.C. Sangster, C. Stoeckl, J.P. Knauer, W. Theobald, K.L. Marshall, M.J. Shoup, T. Buczek, M. Cruz, T. Duffy, M. Romanofsky, M. Fox, A. Pruyne, M.J. Moran, R.A. Lerche, J. McNaney, J.D. Kilkenny, M.J. Eckart, D. Schneider, D. Munro, W. Stoeffl, R. Zacharias, J.J. Haslam, T. Clancy, M. Yeoman, D. Warwas, C.J. Horsfield, J.L. Bourgade, O. Landoas, L. Disdier, G.A. Chandler, R.J. Leeper, The national ignition facility neutron time-of-flight system and its initial performance, Rev. Sci. Instrum. 81 (10) (2010).
[19] M. Cinausero, M. Barbui, G. Prete, V. Rizzi, A. Andrighetto, S. Pesente, D. Fabris, M. Lunardon, G. Nebbia, G. Viesti, S. Moretto, M. Morando, A. Zenoni, F. Bocci, A. Donzella, G. Bonomi, A. Fontana, A proton recoil telescope for neutron spectroscopy, J. Phys. Conf. Ser. 41 (2006) 219–224.
[20] C.C. Lawrence, Neutron spectrum unfolding with organic scintillators for arms-control verification (Ph.D. thesis), The University of Michigan, 2014.
[21] T.J. Langford, C.D. Bass, E.J. Beise, H. Breuer, D.K. Erwin, C.R. Heimbach, J.S. Nico, Fast neutron detection with a segmented spectrometer, Nucl. Instrum. Methods Phys. Res. A 771 (2015) 78–87.
[22] S. Sen, S. Bagchi, R.R. Prasad, D. Venkatasubramanian, P. Mohanakrishnan, R.S. Keshavamurty, A. Haridas, A.J. Arul, P. Puthiyavinayagam, Determination of neutron energy spectrum at KAMINI shielding experiment location, Appl. Radiat. Isot. 115 (2016) 165–171.
[23] N.P. Luciano, A high-energy neutron flux spectra measurement method for the spallation neutron source (Ph.D. thesis), University of Tenessee Knoxville, 2012.
[24] M.A. Mosby, J.W. Engle, K.R. Jackman, F.M. Nortier, E.R. Birnbaum, Determination of spallation neutron flux through spectral adjustment techniques, Nucl. Instrum. Methods Phys. Res. B 381 (2016) 29–33, http://dx.doi.org/10.1016/j.nimb.2016.04.041.
[25] H.R. Vega Carrillo, M.P.I. De La Torre, Catalogue to select the initial guess spectrum during unfolding, Nucl. Instrum. Methods Phys. Res. A 476 (1–2) (2002) 270–272, http://dx.doi.org/10.1016/S0168-9002(01)01467-X.
[26] L. Greenwood, C. Johnson, User Guide for the STAYSL PNNL Suite of Software Tools, PNNL-22253, Tech. rep., Pacific Northwest National Laboratory, 2013.
[27] K.P. Harrig, B.L. Goldblum, J.A. Brown, D.L. Bleuel, L.A. Bernstein, J. Bevins, M. Harasty, T.A. Laplace, E.F. Matthews, Neutron spectroscopy for pulsed beams with frame overlap using a double time-of-flight technique, Nucl. Inst. Methods Phys. Res. A 877 (2018) 359–366, http://dx.doi.org/10.1016/j.nima.2017.09.051.
[28] M. Avrigeanu, A.M. Moro, Improved deuteron elastic breakup energy dependence via the continuum-discretized coupled-channels method, Phys. Rev. C 82 (3) (2010) 1–4.
[29] B.V. Carlson, R. Capote, M. Sin, Elastic and inelastic breakup of deuterons with energy below 100 MeV, 163 (1) (2015) 163–169.
[30] M.A. McMahan, L. Ahle, D.L. Bleuel, L. Bernstein, B.R. Barquest, J. Cerny, L.H. Heilbronn, C.C. Jewett, I. Thompson, B. Wilson, Neutron beams from deuteron breakup at the 88-inch cyclotron at lawrence berkeley national laboratory, Science And Technology (April 2016) (2008) 3–6.
[31] Y. Watanabe, T. Ye, K. Ogata, Analysis of deuteron breakup reactions for energies up to 100 MeV, EPJ Web Conf. 2 (2010).
[32] J. Meulders, P. Leleux, P. Macq, C. Pirart, Fast neutron yields and spectra from targets of varying atomic number bombarded with deuterons from 16 to 50 MeV (for radiobiology and radiotherapy), Phys. Med. Biol. 20 (2) (1975) 235–243.
[33] T. Ye, Y. Watanabe, K. Ogata, Analysis of deuteron breakup reactions on Li7 for energies up to 100 MeV, Phys. Rev. C 80 (1) (2009) 1–8, http://dx.doi.org/10.1103/PhysRevC.80.014604.
[34] K.S. Krane, Introductory Nuclear Physics, John Wiley and Sons, New York, 1988.
[35] M.A. Lone, C.B. Bigham, J.S. Fraser, H.R. Schneider, T.K. Alexander, A.J. Ferguson, A.B. McDonald, Thick target neutron yields and spectral distributions from the 7Li(d,n) and 9Be(d,n) reactions, Nucl. Instrum. Methods 143 (1977) 331–344.
[36] D.L. Bleuel, M.A. McMahan, L. Ahle, B.R. Barquest, J. Cerny, L.H. Heilbronn, C.C. Jewett, Characterization of a tunable quasi-monoenergetic neutron beam from deuteron breakup, Nucl. Instrum. Methods Phys. Res. B 261 (2007) 974–979, http://dx.doi.org/10.1016/j.nimb.2007.04.125.
[37] EG&G ORTEC, MAESTRO for Windows, MCA Emulation Software (A65-BI), 1997.
[38] T.M. Semkow, P.P. Parekh, M. Virgil, Coincidence summing in gamma-ray spectroscopy, 290 (1990) 437–444.
[39] K. Debertin, U. Schotzig, Coincident summing corrections in Ge(Li)-spectrometry at low source-to-detector distances, Nucl. Instrum. Methods 158 (1978) 471–477.
[40] X..M.C. Team, MCNP - a general monte carlo n-particle transport code, version 5, LA-UR-03-1987, 2008.
[41] R. Capote, K. Zolotarev, V. Pronyaev, A. Trkov, Updating and extending the IRDF-2002 dosimetry library, J. ASTM Int. 9 (4) (2012).
[42] F.G. Perey, Least-squares dosimetry unfolding: the program stay'sl (ornl/tm-6062), Tech. rep., Oak Ridge National Laboratory, Oak Ridge, Tennessee, 1977.